

Glyph-based Comparative Visualization for Diffusion Tensor Fields

Changgong Zhang, Thomas Schultz, Kai Lawonn, Elmar Eisemann, and Anna Vilanova

Abstract— Diffusion Tensor Imaging (DTI) is a magnetic resonance imaging modality that enables the in-vivo reconstruction and visualization of fibrous structures. To inspect the local and individual diffusion tensors, glyph-based visualizations are commonly used since they are able to effectively convey full aspects of the diffusion tensor. For several applications it is necessary to compare tensor fields, e.g., to study the effects of acquisition parameters, or to investigate the influence of pathologies on white matter structures. This comparison is commonly done by extracting scalar information out of the tensor fields and then comparing these scalar fields, which leads to a loss of information. If the glyph representation is kept, simple juxtaposition or superposition can be used. However, neither facilitates the identification and interpretation of the differences between the tensor fields. Inspired by the checkerboard style visualization and the superquadric tensor glyph, we design a new glyph to locally visualize differences between two diffusion tensors by combining juxtaposition and explicit encoding. Because tensor scale, anisotropy type, and orientation are related to anatomical information relevant for DTI applications, we focus on visualizing tensor differences in these three aspects. As demonstrated in a user study, our new glyph design allows users to efficiently and effectively identify the tensor differences. We also apply our new glyphs to investigate the differences between DTI datasets of the human brain in two different contexts using different b-values, and to compare datasets from a healthy and HIV-infected subject.

Index Terms—Glyph Design, Comparative Visualization, Diffusion Tensor Field

1 INTRODUCTION

Diffusion-Weighted MRI (DW-MRI) is an imaging technique that exploits the diffusion of water molecules to estimate the underlying anatomical structures of fibrous tissues such as the brain white matter or the muscles. As the only in-vivo imaging modality, it plays a major role in a large number of applications, e.g., the understanding of brain connectivity and development, and the improvement of diagnosis and treatment for brain and muscle diseases. The characteristics of water diffusion can be modeled by a second order tensor called Diffusion Tensor Imaging (DTI) [5]. More advanced DW-MRI acquisition and modeling techniques have been developed in the past decade, such as high angular resolution diffusion imaging (HARDI) [38]. However, DTI remains the preferred DW-MRI modality used in clinical practice.

Apart from analyses based on a single DTI dataset, for some applications it is necessary to analyze two or more DTI datasets. DTI acquisition requires many parameters to be tuned (e.g., the gradient sampling schemes [17, 19] or the b-value [3]), which can affect the estimation of the resulting tensors. In order to better understand the effects of the related parameters, it is helpful to compare the generated DTI datasets. This is also the case for investigating some pathologies (e.g., dyslexia [36]), or the evaluation of DTI registration algorithms [20].

Comparative visualization refers to the process of understanding the differences or similarities between two or more datasets by making use of an easy-to-interpret visual representation. Gleicher et al. [16] presented a general taxonomy that groups visual comparison into three categories: juxtaposition (or side-by-side), superposition (or overlay), and explicit encoding of differences. Juxtaposition is straightforward to implement but relies on the viewers' memory for comparison. Su-

perposition is effective for comparing objects, due to being in the same frame of reference. However, it is likely to cause occlusions and visual clutter. Explicit encoding is effective for visually depicting relationships among objects. However, the information about the original subjects themselves is lost, and the visual representations of the differences are not always intuitive to interpret.

In order to compare two DTI datasets at local level, the tensors are usually reduced to scalar values that have anatomical or physiological meanings. These derived scalar fields are then compared. Fractional anisotropy (FA), for instance, is commonly associated with the integrity of fiber tracts. Their comparison can be performed using common scalar field comparative visualization techniques, e.g., side-by-side visualization [4] or simple quantification of the differences [27]. These are the most commonly used methods for DTI dataset comparison in practice. However, scalar level comparisons reduce the original information, and thus give a limited view of the differences.

Alternatively, the comparison can be performed directly on the tensors. There is less information reduction for tensor level comparisons, and most of the information can be integrally visualized as glyphs. The method commonly employed for direct tensor comparison is to juxtapose the glyphs. For instance, Schultz et al. [35] juxtaposed two groups of glyphs for showing the influence of lower echo time on fiber variance. Superposing glyphs [7, 20] is also used but can be easily affected by occlusion. Da Silva et al. [12] displayed the differences between two DTI datasets by superposing the corresponding streamtubes. However, changing the parameters used for extracting the streamtubes might change the visually perceived differences between the datasets. Therefore, we decided to compare DTI datasets directly at tensor level.

In Figure 1, we illustrate the results of juxtaposition and superposition using two synthetic datasets. Tensor dataset 1 in Figure 1a is defined in the barycentric space of three geometric anisotropy metrics [42]. Tensor dataset 2, as shown in Figure 1b, is constructed by applying a small amount of random variations to tensor dataset 1. Both are visualized via superquadric glyphs [21]. With juxtaposition, the viewers need to compare them mentally, and thus it is hard to distinguish subtle differences. With superposition, it becomes easier to identify whether two tensors are different or not, if their sizes are comparable. If not, one could be totally enclosed in the other. Occlusion is another problem when simply superposing glyphs. An option to address the occlusion problem is using transparency. However, subtle differences still remain unclear, as shown in Figure 1d. In all the meth-

-
- Changgong Zhang, Elmar Eisemann, and Anna Vilanova are with Computer Graphics and Visualization Group at Delft University of Technology. E-mail: {c.zhang-3,e.eisemann,a.vilanova}@tudelft.nl.
 - Thomas Schultz is with Visualization and Medical Image Analysis Group at University of Bonn. E-mail: schultz@cs.uni-bonn.de.
 - Kai Lawonn is with Visualization Group at University of Magdeburg and Computer Graphics and Visualization Group at Delft University of Technology. E-mail: lawonn@isg.cs.uni-magdeburg.de.

Manuscript received 31 Mar. 2015; accepted 1 Aug. 2015; date of publication xx Aug. 2015; date of current version 25 Oct. 2015.

For information on obtaining reprints of this article, please send e-mail to: tvcg@computer.org.

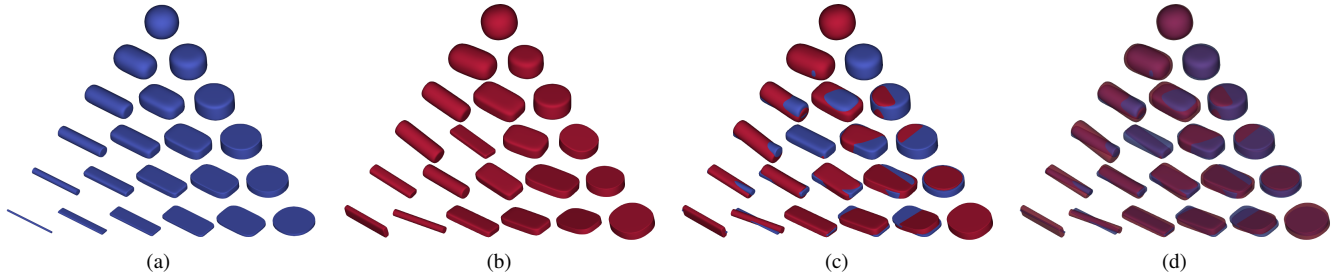


Fig. 1. Different visual comparisons for two synthetic datasets. (a & b) juxtaposition, (c) superposition, and (d) superposition with transparency.

ods mentioned above, the differences are *integrally* perceived rather than *separately* characterized. In other words, even if it is easy to tell whether or not two tensors are different, it is hard to tell, for example, which factor contributes most to the overall perceived difference.

The symmetric second-order positive-definite diffusion tensor can be decomposed into three components, which are tensor scale, shape, and orientation in the context of tensor glyph design [14, 34]. These components define the whole tensor and give an intuitive interpretation. In order to support the individual comparison of these three tensor components, we design a glyph to present tensor differences in scale, shape, and orientation *separately*. To the best of our knowledge, there are no glyph-based methods for comparative visualization of two diffusion tensor fields that go beyond juxtaposition or superposition.

In this work, we focus on the tensor comparison at local level and present the *Tensor difference (Tender)* glyph to efficiently represent the differences between two diffusion tensor fields based on the three components (i.e., scale, shape, and orientation). The Tender glyph is inspired by the checkerboard style visualization [37] and the superquadric tensor glyph [21]. Checkerboard visualization, a type of juxtaposed visual comparison, is frequently used to evaluate registration accuracy [25]. Differences result in obvious discontinuities along the checkerboard edges, which can be easily perceived. The superquadric tensor glyph generates a strong visual cue for tensor shape and orientation via sharp edges, and largely reduces visual ambiguity.

The main contributions of this work are:

- A novel glyph design, encoding differences between two diffusion tensors in terms of scale, shape, and orientation which facilitates visual comparison.
- A tensor dissimilarity measure and the associated feature space to explore the differences between two diffusion tensor fields.

Furthermore, we present a user study and two cases where we illustrate the potential applicability of the Tender glyph.

2 RELATED WORK

The presented work is in the field of glyph-based visualization, which is a common and creative form of visual design. Its major strength is the ability to visually encode multivariate dataset in the spatial context. Glyph-based visualization for DW-MRI as well as comparative visualization literatures are described in this section.

2.1 Glyph-based Visualization

Glyph-based visualization enables the visual representation of multivariate data by encoding them into various visual channels (e.g., color, size, shape). Compared to other visualization techniques for multivariate data, such as parallel coordinate plots, glyph-based visualization can preserve the spatial context. Due to the inherent multivariate characteristic of diffusion tensors, glyphs are commonly used to visualize DTI datasets. The classic way is to employ ellipsoids [28, 31]. Westin et al. [41] designed a composite glyph to directly show the linear, planar, and spherical components. Kindlmann [21] proposed the superquadric glyph to improve the visual perception and to reduce image space ambiguity. Schultz and Kindlmann [34] proposed several

general principles for glyph-based visualization for symmetric tensor data including the preservation of symmetry, continuity, and disambiguity. Ropinski et al. [32] presented a survey of some representative glyph designs and the taxonomy of glyph properties for spatial multivariate medical data. Borgo et al. [8] proposed general glyph design criteria and guidelines to help facilitate the effective design of glyph-based visualization.

2.2 Comparative Visualization

Visualization techniques have been developed to facilitate comparative data analysis in scientific research. Busking et al. [9] proposed an image-based implementation to visually compare two intersecting surfaces by local distance cues (e.g., fogging) and contours. van Pelt et al. [39] presented an intuitive details-on-demand glyph set for comparatively visualizing wall-shear stresses between different stent configurations. Schmidt et al. [33] introduced a comparative visual analysis system for multiple 3D meshes that combines explicit encoding, juxtaposition, and parallel coordinate plots for quantitative measures.

However, few methods are designed specifically for diffusion tensor fields. The most common approach to compare subjects in DTI visualization is to place the resulting images side-by-side. Hotz et al. [18] compared the results of two tensor interpolation approaches by juxtaposition. The comparison in quantitative DTI image analysis is more often performed discarding the spatial information. Line charts or scatter plots of relevant scalar-valued invariants are commonly juxtaposed and/or superposed for comparison [13]. Parallel to our work, Abbasloo et al. [1] developed a framework to visualize the voxel-wise normal distribution of diffusion tensors. They compared two diffusion tensors by superposition. They intended to avoid the occlusion problem by rendering them in complementary colors, and adding the resulting images. However, the rest of the issues about superposition presented before remain.

To the best of our knowledge, no glyph-based technique has been presented that provides comparative visualization of two DTI fields based on *explicit encoding* of differences.

2.3 Tensor Dissimilarity Measure

An important challenge in the data level comparison approach is to design suitable metrics for the data compared [40]. In our case, the metric means the tensor dissimilarity measure, which is also an important factor in tensor field segmentation [26].

There is no unique way to calculate the distance between tensors. In literature, several measures have been proposed to calculate the similarity or distance between tensors, see Peeters et al. [30]. An easy to compute and widely used measure is the Frobenius norm, which can be applied to all types of tensors. Other metrics have been proposed specifically for symmetric and strictly positive definite tensors, such as the Riemannian metric [15] or the log-Euclidean approach [2]. Kindlmann et al. [23] proposed a measure built on the geodesic-loxodrome that divides the overall distance into components that have intuitive meanings for DTI (i.e., shape-specific and orientation-specific distances). The fact that these measures produce intuitive distance components makes it an interesting choice for our glyph design.

3 GLYPH DESIGN

The goal of our glyph design is to help the users gain insight into the differences between two diffusion tensors beyond what a simple juxtaposition or superposition can provide. The first step to build the glyph is to analyze the tasks we want to achieve by comparing two DTI datasets. Based on this analysis, a selection of dissimilarity measures is done, and these measures are encoded into various visual channels of the glyph. In this section, we present the whole design process.

3.1 Task Analysis

Before starting the design process, we must decide what kind of information is useful for comparing two diffusion tensor fields. In DTI, diffusion scale (e.g., mean diffusivity, MD) represents the overall diffusion extent. Consistent increases in MD in some fiber tracts may indicate white matter degeneration [13]. The diffusion anisotropy type is useful to identify the underlying fibrous structure patterns. In single fiber areas such as the corpus callosum, the diffusion has a clearly defined principle diffusion direction (i.e., linear anisotropy), while in fiber crossing areas such as the centrum semiovale, the diffusion type is more like a flat disc (i.e., planar anisotropy). Since diffusion scale and anisotropy do not depend on orientation, they are rotationally invariant. If a tensor is not spherical, its diffusion orientation can be defined. The orientation is important for the reconstruction of fiber tracts, which represent the underlying white matter structures. Therefore, we decided to divide the differences into diffusion scale, shape, and orientation. These components are orthogonal to each other [22], e.g., a change in orientation will not cause a change in shape.

Furthermore, we adopt two glyph design principles, which are continuity and disambiguity [34]. The glyph for two distinct tensors should emphasize the visual representation, while the glyph for two nearly equal tensors should not. Disambiguity means that the shapes of two distinctive tensors should be clearly distinguishable, and as independent of the viewing direction as possible. In this work, we also employ the superquadric glyph, which can guarantee unambiguous perception and at the same time preserve continuity. Some properties of the superquadric glyph can be found in Kindlmann [21] and Demiralp et al. [10]. To achieve our goal, the glyphs should also be able to provide information about the amount of differences of the three components (i.e., scale, shape, and orientation) *independently*.

3.2 Tensor Dissimilarity Measure

In order to define the dissimilarity measure, we decompose a diffusion tensor in a similar way to Schultz and Kindlmann [34]. A symmetric second-order positive-definite tensor \mathbf{T} can be decomposed to three ordered real eigenvalues $\{\lambda_1 \geq \lambda_2 \geq \lambda_3\}$. The Frobenius norm of a tensor is defined as $\|\mathbf{T}\| = \sqrt{\sum_i \lambda_i^2}$. Notice that the Frobenius norm is rotationally invariant, as are the eigenvalues. Then we get the normalized tensor $\tilde{\mathbf{T}} = \mathbf{T}/\|\mathbf{T}\|$ and the normalized eigenvalues $\tilde{\lambda}_i = \lambda_i/\|\mathbf{T}\|$.

The Frobenius norm represents the overall diffusion scale, while the set of three normalized ordered eigenvalues $\{\tilde{\lambda}_i\}$ represents the diffusion anisotropy type. The set of three orthonormal eigenvectors $\{\mathbf{e}_i\}$ represents the diffusion orientation. We define the tensor dissimilarity measures between two tensors $\mathbf{T}^{(1)}$ and $\mathbf{T}^{(2)}$ as:

$$d_s(\mathbf{T}^{(1)}, \mathbf{T}^{(2)}) = \left| \|\mathbf{T}^{(1)}\| - \|\mathbf{T}^{(2)}\| \right| \quad (1)$$

$$\tilde{d}(\mathbf{T}^{(1)}, \mathbf{T}^{(2)}) = \|\tilde{\mathbf{T}}^{(1)} - \tilde{\mathbf{T}}^{(2)}\| \quad (2)$$

$$d_{sh}(\mathbf{T}^{(1)}, \mathbf{T}^{(2)}) = \sqrt{\sum (\tilde{\lambda}_i^{(1)} - \tilde{\lambda}_i^{(2)})^2} \quad (3)$$

$$d_o^2(\mathbf{T}^{(1)}, \mathbf{T}^{(2)}) = \tilde{d}^2 - d_{sh}^2 \quad (4)$$

where d_s is the scale difference, \tilde{d} is the normalized tensor difference, d_{sh} is the shape difference, and d_o is the orientation difference.

The main idea is based on the Pythagorean theorem. The difference between two normalized diffusion tensors can only be due to the shape and/or orientation difference. If we subtract the shape difference from the normalized difference, the orientation difference remains. Note that \tilde{d} could also be defined as the ‘angle’ between two normalized tensors $\tilde{d} = \arccos(\tilde{\mathbf{T}}^{(1)} : \tilde{\mathbf{T}}^{(2)})$ (The ‘:’ operator denotes a tensor contraction). If so, d_{sh} should also be defined as the ‘angle’ between two sets of normalized eigenvalues $d_{sh} = \arccos\left(\sum (\tilde{\lambda}_i^{(1)} \tilde{\lambda}_i^{(2)})\right)$. Numerically, these definitions make little differences.

The advantage of these measures is that they are easy to calculate, intuitive, and fulfill our requirements. For instance, the orientation distance between an isotropic (i.e., spherical) tensor and a linear-anisotropic tensor is zero. The orientation difference between linear and planar anisotropy is the largest if the orientation of the linear tensor is perpendicular to the plane defined by the planar anisotropy. Furthermore, shape difference and orientation difference are bounded. Using the geodesic-loxodromes [23] as the dissimilarity measure would also provide the desired characteristics for our glyph design. However, the computational cost of calculating the geodesics is considerably high, so we opt for the computationally simpler alternative presented here.

3.3 Visual Mapping

Once the three components of the tensor differences are computed as described in the previous subsection, we encode them to various visual channels that constitute the Tender glyph.

Shape Difference Encoding Following the design guideline of intuitive mapping based on semantics [8], the shape difference d_{sh} can be encoded into the shape channel of the glyph. However, expressed as a single scalar value, it gives little information concerning the characteristics of the shape change. For instance, d_{sh} can be the same between isotropy and linear anisotropy as well as planar and linear anisotropy. It is not easy to connect these back to the original tensor shapes. Therefore, we do not use an explicit encoding of the shape differences. Instead, we preserve the original tensor shapes as much as possible while still facilitating their visual comparison.

Tensor shape is scale-invariant because shape and scale are orthogonal. Thus, we normalize both tensors before shape comparison. We also observed that it is hard to identify the shape differences in terms of three eigenvalues when two tensor glyphs have different orientations. For instance, as shown in Figure 2a, two tensors are with unit scale but different orientations and shapes. No matter how we compare them, by juxtaposition (Figure 2a) or by superposition (Figure 2b bottom), it is difficult to identify the shape differences by sight. As soon as we align them to the orientation of one of these two tensor glyphs (Figure 2b top), it becomes easier to tell which tensor has larger or smaller eigenvalues. However, occlusion still makes it hard to judge the extent of shape differences. Transparency is used to handle occlusion (Figure 2c), but it remains hard to visually quantify the shape differences.

Inspired by the checkerboard visualization, we explain our idea in 2D in Figure 3a. One of the superquadric glyphs is first aligned with the other (see Figure 3b). Therefore, we can maintain the original orientation of one tensor. Then, we divide the 2D space into four quadrants (i.e., eight parts in 3D), each bounded by two half-axes displayed as dotted black lines in Figure 3c, like a checkerboard. We alternate the displaying of the corresponding parts of superquadric glyphs in each quadrant. Figure 3d shows the corresponding 3D case. If two tensors have similar shapes, there will be no significant changes along the axes. Otherwise, abrupt changes appear which are easy to recognize. The traditional checkerboard visualization introduces information loss due to its characteristic of alternative displaying. However, there is no shape-specific information loss in our case, since both the tensor and the superquadric glyphs are symmetric and one octant contains all information. Furthermore, we still keep the sharp edges, which serve as strong visual cues for orientation and shape [21]. Note that the use of orthographic projection is necessary since the shape comparison relies on the correct perception of length differences along the axes.

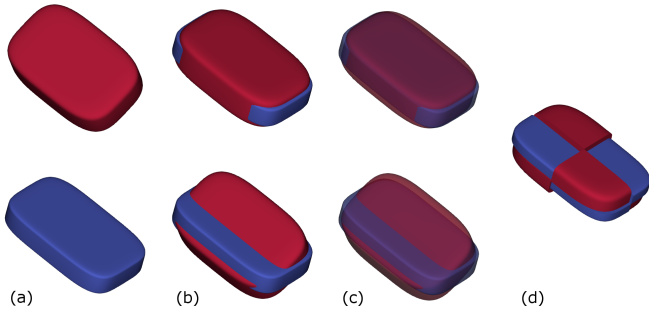


Fig. 2. The Tender glyph shows the shape difference between two tensors of unit scale but with different orientations. (a) shows two tensor glyphs placed side-by-side. (b) bottom shows them overlaid. (b) top shows them overlaid, but the red glyph is aligned with the blue one. (c) superposition with transparency. (d) the Tender glyph. The differences in terms of three eigenvalues are more obviously manifested by the “staircases” between two parts of the Tender glyph.

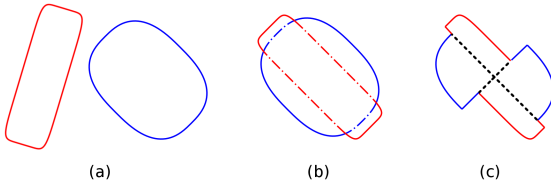


Fig. 3. 2D Illustration of the checkerboard style glyph design. (a) shows two 2D glyphs side-by-side. (b) shows them overlaid but the red glyph is aligned with the blue one. The solid lines represent the visible parts while the dash-dot lines are the invisible parts due to occlusion. (c) shows the result of our design. The two black dot lines divide the 2D space into four parts. Two glyphs are displayed alternatively. There are obvious discontinuities between two glyphs.

Scale Difference Encoding In the context of DTI, tensor scale is interpreted as the ‘size’, representing the amount of diffusion. It is intuitive to encode the scale difference d_s to the size channel of the Tender glyph. However, in this way, it is impossible to tell which tensor has a larger or smaller scale. An alternative is to directly map the original tensor scale $\|\mathbf{T}\|$ to the size of its corresponding part of the checkerboard superquadrics. However, these mappings do pose a problem for the perception of tensor scale. The superquadric glyph inherently introduces volume differences for tensors with the same Frobenius norm, but with different shapes. It is difficult to isolate the diffusion scale differences. Therefore, we decided to encode either the individual tensor scales $\|\mathbf{T}^{(i)}\|$ or the scale differences d_s into color.

Encoding individual tensor scales enables voxel-wise scale comparison, while encoding scale differences can facilitate the comparison across the field. Additionally, we design two colormaps for scale information encoding. We use the same tensor datasets as shown in Figure 1 for illustration. The dual hue colormap is used to show individual tensor scales (see Figure 4a). Hue, as an effective categorical cue, is used to distinguish tensor datasets. Scale information is reflected by color luminance. Perceptually, it is easier to compare color luminance than to evaluate size differences when shapes vary. However, it is hard to compare the subtle luminance differences of two colors with different hues for a given voxel (see Figure 4a). Thus, we introduce the single hue colormap (see Figure 4b). It facilitates detecting subtle luminance differences for both local individual scales and scale differences across the field (see Figure 4d). Colors of the same hue can facilitate the comparison of luminance. Glyph halos are then added for distinguishing datasets. Similarly, Chung et al. [11] used outline color for distinguishing home or opposition teams in the visual analysis of rugby events.

When encoding the scale differences d_s , the Tender glyph has the same hue and luminance for all octants, and it becomes harder to iden-

tify the differences in shapes (see Figure 4d). Switching to the dual hue colormap improves the combined perception of scale differences and shape differences (see Figure 4c). Therefore, the single hue colormap together with the halos is mainly for more accurate scale comparisons, while the dual hue colormap is for the combined perception of scale differences and shape differences simultaneously.

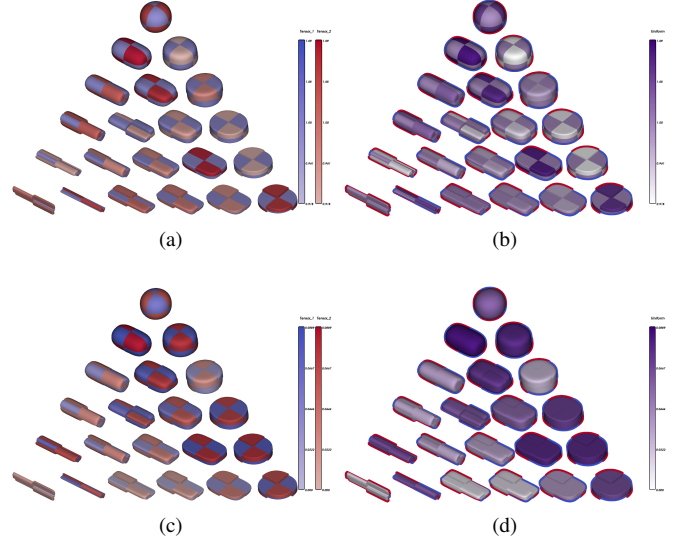


Fig. 4. Two scale encoding schemes and two colormaps. (a) and (b) show that individual tensor scales $\|\mathbf{T}^{(i)}\|$ are color-encoded with the dual hue and the single hue colormaps, respectively. This encoding scheme is suitable for local voxel-wise scale comparison. (c) and (d) show that tensor scale differences d_s are color-encoded with the dual hue and the single hue colormaps, respectively. This encoding scheme is suitable for scale comparison across the field. The single hue colormap is for more accurate comparison while the dual hue colormap is for combined perception of scale and shape differences simultaneously.

Orientation Difference Encoding The orientation of a diffusion tensor is represented by its three eigenvectors. Straightforward visualization of two sets of eigenvectors as vectors has several disadvantages. The differences between them are not easily perceived due to their 3D nature. More importantly, eigenvectors cannot be uniquely defined for tensors of certain shape types. Therefore, we decided to explicitly encode the scalar-valued orientation difference d_o , which is semantically mapped to the open angle of a view-aligned arc.

Given two perfectly linear-anisotropic tensors $\mathbf{T}^{(1)} = \mathbf{T}^{(2)} = [1\ 0\ 0; 0\ 0\ 0; 0\ 0\ 0]$ (FA = 1.0, mode = 1.0 [14]) aligned with each other, if we gradually rotate tensor one $\mathbf{T}^{(1)}$ around vector (0, 0, 1) from 0° to 180° while keeping tensor two $\mathbf{T}^{(2)}$ fixed, the analytical behavior of the orientation difference is $d_o = \sqrt{2}\sin(\theta)$ with θ the rotation angle, shown as the red curve in Figure 6.

For simplicity, we approximate it with a quadratic curve (see the green curve in Figure 6). Then, the mapping from d_o to θ is

$$\theta = 90^\circ \left(1 - \sqrt{1 - \sqrt{2}d_o/2} \right).$$

If tensors are not perfectly linear-anisotropic, their orientation difference for the same rotation angle will be smaller. As an example, the blue dots in Figure 5 indicate the values for $\mathbf{T}^{(1)} = \mathbf{T}^{(2)} = [0.99\ 0\ 0; 0\ 0.1\ 0; 0\ 0.1\ 0]$ (FA = 0.89, mode = 1.0 [14]). Figure 5a shows the tensors used in this experiment, and the corresponding arcs are shown in Figure 5b. Note that the left- and right-most arcs disappear since there are no orientation differences, which meets the requirements of continuity. Figure 5c illustrates the arcs for the case of two perfectly linear-anisotropic tensors.

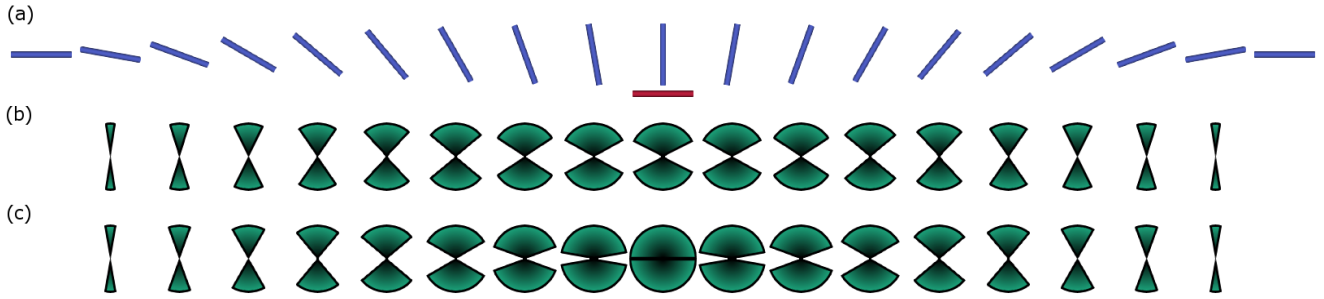


Fig. 5. The arcs for encoding orientation differences. (a) shows a group of linear tensors with gradually varying orientations (blue) and a reference tensor (red), and (b) shows the corresponding arcs for the orientation differences between each element tensor with the reference. (c) shows the results for two perfectly linear-anisotropic tensors in the same manner.

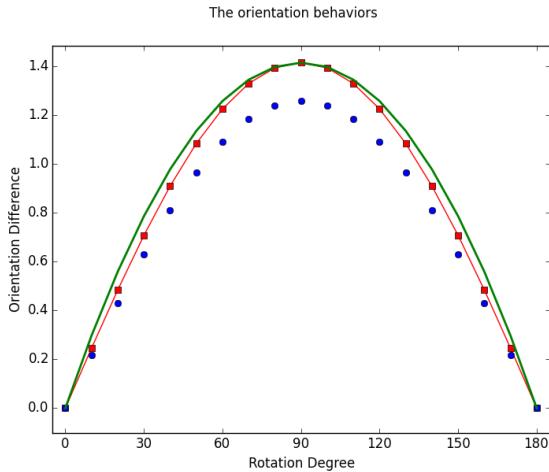


Fig. 6. The red curve and squares together show the analytic behavior of d_o between two perfectly linear-anisotropic tensors with respect to the rotation angle. The green curve is the quadratic approximation. Blue dots are d_o of other two linear-anisotropic tensors with reduced FA.

In a second experiment, we demonstrate that the orientation difference metric d_o does not measure a spurious orientation difference in cases where one of the tensors is isotropic. To this end, we select $\mathbf{T}^{(1)} = [0.94 \ 0 \ 0; 0 \ 0.24 \ 0; 0 \ 0.24 \ 0]$, $\mathbf{T}^{(2)} = [0.24 \ 0 \ 0; 0 \ 0.94 \ 0; 0 \ 0.24 \ 0]$. We keep tensor one $\mathbf{T}^{(1)}$ fixed, and gradually change tensor two $\mathbf{T}^{(2)}$ to a spherical tensor by reducing its FA to 0 while preserving the scale and mode [14], as shown in Figure 7. The open angle of the arc gradually reduces to 0. This experiment again confirms the continuity of our orientation difference metric.

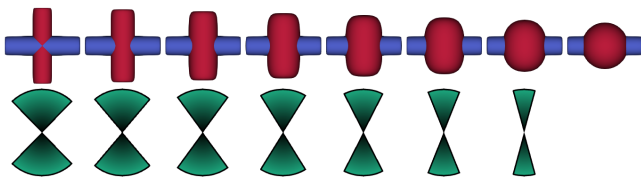


Fig. 7. The behavior of d_o when reducing the FA of one linear-anisotropic tensor (the red one) to 0 while keeping the other (the blue one) fixed. Both are of unit scales. The open angle of the arc gradually decreases until it disappears.

Since the possible maximum of the normalized eigenvalue $\tilde{\lambda}_1$ is one, the radius of the arc is set to be slightly larger than one in order to maintain its visibility. Within certain ranges of viewpoints, those arcs could overlap. Thus, similar to Lie et al. [29], we add an eye-space fixed-width outline to support the depth perception and individ-

ual identification. Our final design is achieved by adding the checkerboard style superquadrics, scale-encoded color channels, and the view-aligned arc for orientation differences together, as shown in Figure 8a. The Tender glyphs are applied to visualize the differences between the same synthetic datasets used in Figure 1. The dual hue colormap is used to encode individual tensor scales.

4 GLYPH VISUALIZATION

If the glyphs are placed throughout the whole volume, they probably occlude each other and cause visual clutter. Thus, glyph-based techniques are more suited for 2D and/or sparse visualization. In this work we place the glyphs at one or more selected slices. Furthermore, users can restrict the display of the glyphs at anatomically meaningful structures of interest (e.g., corpus callosum). A smart glyph arrangement strategy [24] can remove the distracting effects of the regular sampling grid. However, this approach requires diffusion tensor interpolation. Therefore, we decided to place the glyphs at the original grid points.

Since the Tender glyph does not have an intrinsic orientation, we develop various strategies for its orientation. The options include *a)* aligned with DTI dataset 1; *b)* aligned with DTI dataset 2; *c)* view-aligned oblique view; *d)* view-aligned projection of any pair of two eigenvalues. Aligning the glyphs with respect to one of the datasets is useful when preserving the original orientations are important. An oblique view is good to provide the first impression of the differences of all the three eigenvalues, while the projection of any two eigenvalues can support more accurate comparisons. How the Tender glyphs look like with these orientation strategies can be seen in Figure 8. Furthermore, we introduce an interaction for manipulating the glyphs, which is termed as *independent rotation*. The glyphs can be freely rotated around their own centers for a better perception of the shape differences without changing the current camera settings.

To facilitate exploration, we incorporate the visualization of a feature space. It uses as features: scale difference d_s , shape difference d_{sh} , orientation difference d_o , normalized tensor difference \tilde{d} and the Frobenius norm of the difference tensor $d_F = \|\mathbf{T}^{(1)} - \mathbf{T}^{(2)}\|$. The scatter plot matrix (SPLOM) approach is used to arrange the visualizations of these features (see Figure 9). Three histograms, placed at the main diagonal, show the distributions of d_s , d_{sh} , and d_o , while the histograms of \tilde{d} and d_F are shown at the upper diagonal. Logarithmic scale is used for all the histograms. Three scatter plots at the lower triangular part show the relationship between any pair of the features d_s , d_{sh} and d_o . For each scatter plot, a density map generated from the whole dataset serves as the context, while the green dots drawn on top represent the distribution of the currently selected tensors. Linked views with filtering are used to support interactive exploration.

5 IMPLEMENTATION

We implement our prototype as a plug-in for *vIST/e*¹ in the C++ programming language. The Visualization Toolkit (VTK), OpenGL library, and GLSL shading language are used as developing tools.

¹<http://sourceforge.net/projects/viste/>

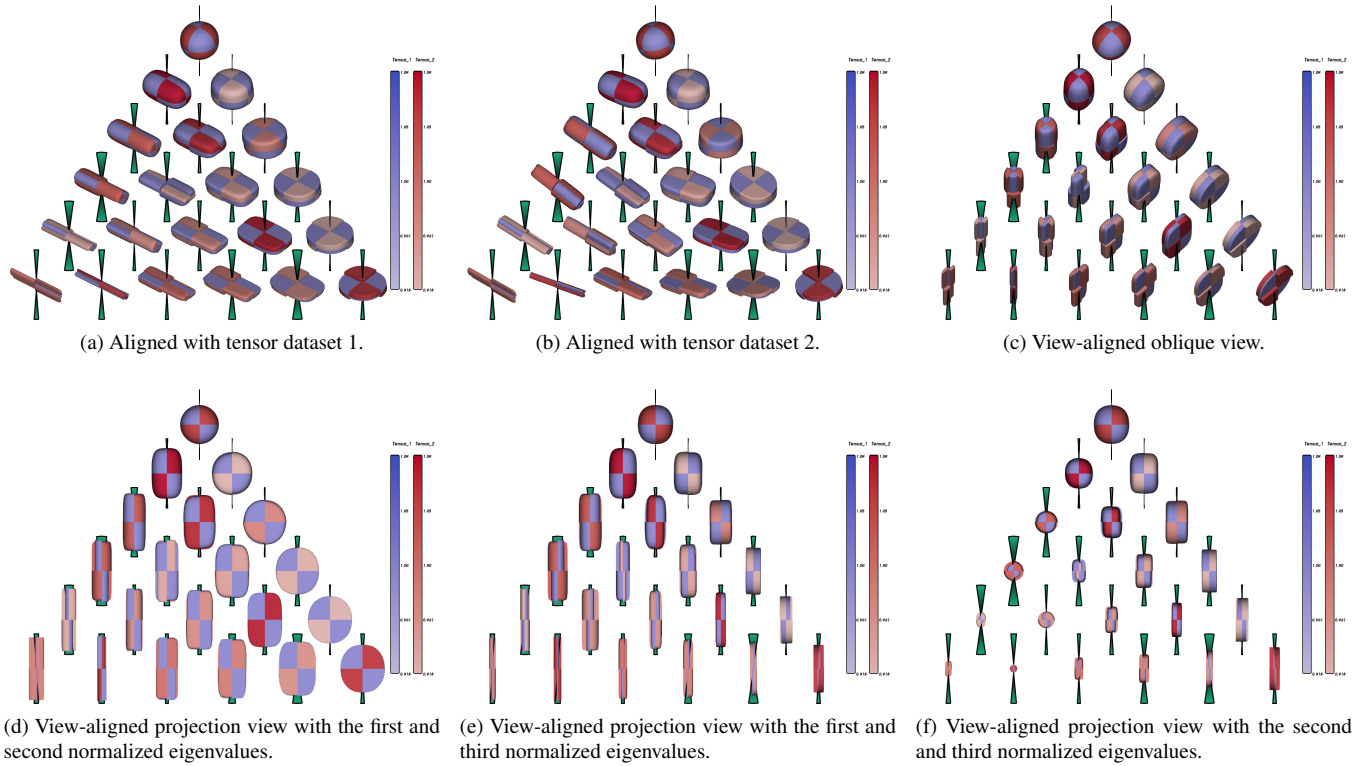


Fig. 8. Various strategies for orienting the Tender glyphs in 3D space.

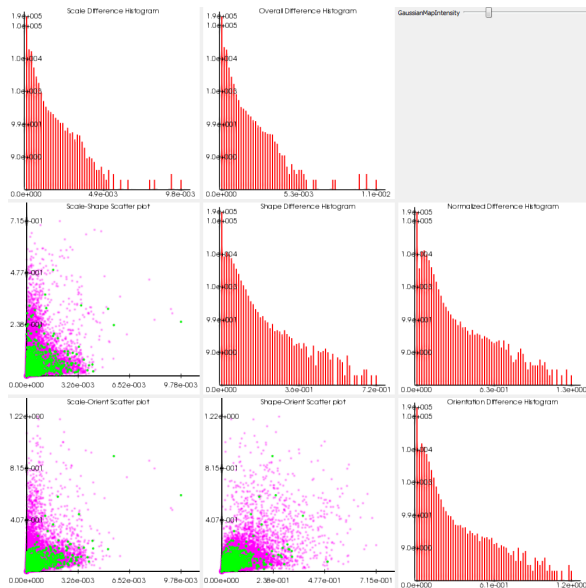


Fig. 9. The feature space is composed of three scatter plots and five histograms. Three scatter plots are for the relationship of any pair of the features d_s , d_{sh} , and d_o . Five histograms are for d_s , d_{sh} , d_o , \bar{d} , and d_F .

The geometries of the checkerboard-style superquadrics are constructed via a precomputed palette of base superquadric shapes [34]. In order to save graphics card memory, we only construct one eighth of each of the possible glyph geometries due to inherent symmetry. The total number of geometries for the precomputed palette is 231, which is enough for our goal. The vertex positions and the normals are stored in card memory. During rendering, the base geometry is used four times to generate the checkerboard-styled superquadrics for

each tensor with its corresponding transformation matrix. Phong shading is employed to support the perception of the shapes. The halos are rendered in a similar way to Schultz and Kindmann [34].

The arc of the Tender glyph is built in the geometry and fragment shaders. A view-aligned quad is generated at each seeding point and texture coordinates are assigned to each corner for subsequent processing to obtain the expected open angle. 4×4 multi-sampling is implemented to relieve the aliasing problem for the outline. Since the arc is analytically generated, the associated attributes for extra samples are computed in the fragment shader. This does not introduce any noticeable performance loss.

6 USER STUDY

We conducted an initial user study in order to find out whether our requirements have been achieved by the Tender glyph. Since we intended to evaluate the effectiveness and efficiency of the glyph design on its own, the feature space was not included in the study. To be able to include more users, we abstracted from the diffusion-related concepts. We had 13 participants with various backgrounds: computer science (10; among them, 6 have experiences with computer graphics), DTI image analysis (2), and applied mathematics (1). The evaluation, which took 90 minutes on average per participant, consisted of three phases. In the first phase, we explained the three components on which the Tender glyph is based, i.e., scale, shape, and orientation. We also introduced the juxtaposition/superposition comparison techniques as well as superposition combined with transparency. 6 out of 13 did the test with all the three visualization methods while the rest did without the superposition plus transparency. Finally, we demonstrated our design in a live demo with our prototype. In the second phase, the participants themselves tried both the Tender glyph, the juxtaposed/superposed glyph, and the transparent superposed glyph to get used to the visualization as well as the available interactions. In the third phase, 22 or 33 controlled tests were performed depending on whether the superposition with transparency test was added or not. During each test, the participants had to perform a comparison task and answer one to three questions as fast and accurately as possible.

For all tests except the last three, two datasets each with 8 tensors were present, forming 8 tensor pairs. Participants needed to pick one or more pairs out of these 8 pairs as the answer. For example, they needed to find out which pairs have the smallest shape differences or the largest orientation differences. For the last three tests, they had to answer similar questions but with relatively large fields (9×9). In order to correctly measure their accuracy in answering these questions, we allowed them to give no answer when they were uncertain. One of the three glyph-based methods was randomly assigned to visualize the differences between the test datasets. None of the test datasets was repeated for the same participant. Each test dataset appeared only once during the whole phase. In the end, open questions designed to collect their impression on the utility of our design were asked. An overall ranking on a scale from 0 to 10 about the usefulness of the juxtaposition/superposition, superposition with transparency, and the Tender glyph was asked as the last question.

There were 8, 4 and 8 questions asked for the comparison of orientation, shape, and scale, respectively. The accuracy and efficiency (i.e., time) results of orientation difference comparison tests are shown as two boxplots in Figure 10a and 10b. In general, they achieved better results with much less time using the Tender glyph. The results confirm that the perception of orientation differences in terms of open angles is easy to spot and interpret. The accuracy and efficiency of shape-related questions are shown in Figure 10c and 10d. In terms of accuracy, the results indicate that the Tender glyph provides more accurate results, while in terms of efficiency there are no significant differences among all the methods. Four participants stated in the open questions that all the methods worked equally well for the shape comparison, so they had no preference. But it is interesting to observe that they improved the accuracy and spent less time with the Tender glyph, despite their perception. There was one participant who correctly answered all the shape-related questions with both transparent superposition and the Tender glyph. But this participant spent less time with the Tender glyph (140s < 177s), and also mentioned in the open questions that the checkerboard design provides stronger visual cues for shape differences, making them easier to recognize. The results for scale comparison are shown in Figure 10e and 10f. In terms of accuracy, the results do not clearly indicate whether Tender glyphs or superposition with transparency is superior. The efficiency is clearly better with superposition plus transparency. 5 out of 6 participants mentioned that for small field comparisons they preferred superposition plus transparency since they could roughly estimate the scale differences, as well as decide which tensor has a large or small scale for a specific pair simultaneously. Using the Tender glyphs to obtain the same information requires extra interactions, which causes a more time-consuming exploration. For large field comparisons, they all agreed that it is easier with the colormap-based encoding scheme. In practice, many comparisons would be performed on large fields, as shown in the following two case studies. We also realized that the complexity of the interface and the interaction with the prototype creates a steep learning curve for novice users of the Tender glyph. An interesting statement from one participant with DTI image analysis background was that the dual hue colormap is counter-intuitive since blue represents low values in the rainbow colormap that is commonly used in his research.

The results of the questions, in relation to the preferences, are as follows. The average ranking for superposition is 4.5. This method could cause occlusions, which makes the comparisons more difficult. They gave 5 on average for juxtaposition. In this way, they could perceive full information which is helpful for rough comparisons in a small field. For accurate comparisons, especially in a large field, it is difficult to mentally match the corresponding tensor glyphs for comparison. They gave 6.2 on average for superposition with transparency. The advantage of this method is that the occlusion problem and the matching problem are relieved. But there are no strong visual cues for shape comparison. Furthermore, for orientation comparison they had to mentally imagine how to align two glyphs in order to deduce the orientation difference. They gave 7.8 on average for the Tender glyph. With the Tender glyph, the orientation comparison is easy to perform. The Tender glyph also provides stronger visual cues for shape com-

parison than other glyph-based methods. For scale comparison, several participants suggested that we should simplify the user interface to make it simpler to learn. Furthermore, one participant with DTI image analysis background suggested that the Tender glyph is useful when to avoid presenting and looking at several tensor scalar images next to each other. With the Tender glyph, one image, containing all the information about the tensor differences, would be sufficient.

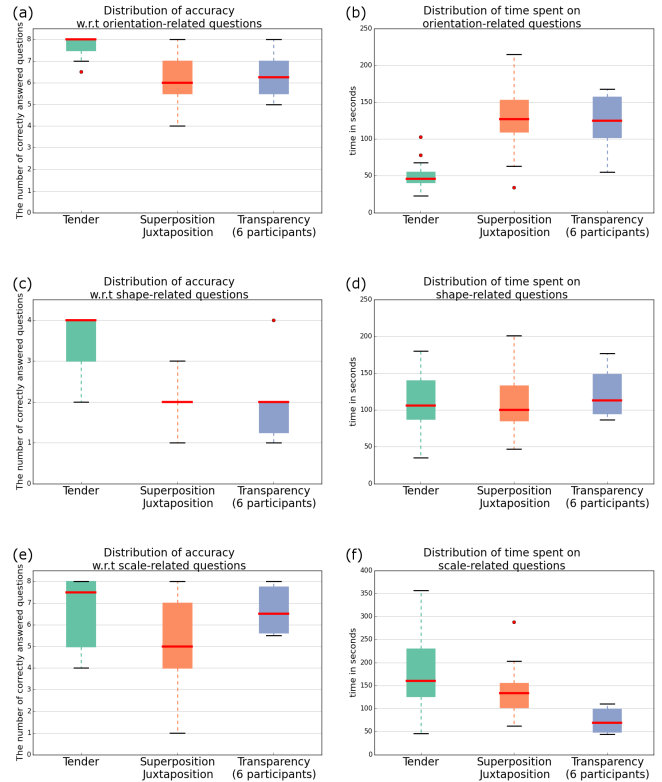


Fig. 10. The results of the user study in terms of accuracy and efficiency. (a), (c), and (e) represent results in terms of accuracy, while (b), (d), and (f) represent results in terms of efficiency for comparison tasks related to orientation, shape, and scale differences, respectively.

7 CASE STUDY

One of the main applications of DTI is the imaging of white matter in the brain. DTI has the potential to provide better understanding of brain connectivity, and improve diagnosis and treatment of diseases such as HIV [43]. Comparison of diffusion tensor fields is part of the analysis to achieve these goals, e.g., to compare the results of different acquisition settings to optimize acquisition sequences, or to compare datasets to find markers that can distinguish pathological tissues.

The main idea of the Tender glyph is to improve the ability to visually reveal local tensor differences as well as large scale patterns in the datasets. Furthermore, by linked selection of the associated feature space, interesting pattern identification is facilitated. In this section, we illustrate the application of Tender glyphs in two scenarios where two DTI datasets are compared.

B-value is an important parameter in DTI acquisition that defines a trade-off between signal-to-noise ratio and contrast. It is often unknown what exact output a b-value change will produce. Two DTI datasets of the same subject, acquired with a b-value of 1000 and 2000 respectively, are compared. The size is $80 \times 80 \times 38$ at $2.875 \times 2.875 \times 3mm$ resolution. A coronal slice is shown in Figure 11a. Blue corresponds to the b-value 1000 DTI dataset, while red represents the b-value 2000 one. It can be immediately observed that only the left bottom and right bottom areas of the slice show large differences in orientation. Figure 11b shows the superposition of the

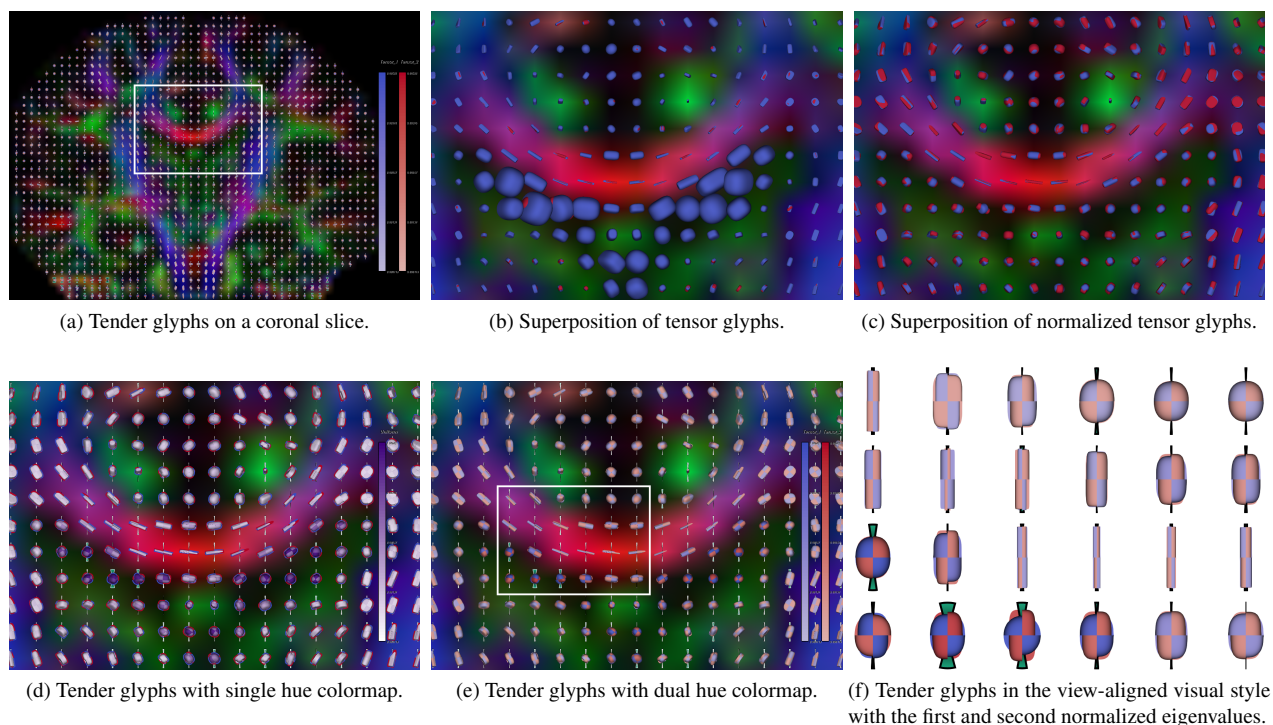


Fig. 11. The application of the Tender glyphs to compare two DTI datasets acquired with different b-values.

superquadratic glyphs without normalization in the area marked with a rectangle in Figure 11a. Due to large variations in tensor scales, most of the red glyphs are enclosed by the blue ones. Figure 11c shows the superposition of normalized glyphs. Since they occlude each other, it is hard to distinguish their shape and orientation differences. Moreover, the exact tensor scale differences are impossible to deduce after normalization. Figure 11d visualizes the tensor differences with the Tender glyphs. The voxels with the largest orientation differences (i.e., the largest open angles) can be quickly spotted via the arcs of the Tender glyphs, indicating their pre-attentive capabilities. Most of the open angles of the arcs are very small, which reveals that the orientation differences are quite little within this area. The individual tensor scales are encoded via the single hue colormap. By comparing lightness, the extent of scale differences can be estimated. The halos around the glyphs help to identify the corresponding DTI dataset. The single hue colormap together with the halos clearly show that the tensors from the DTI dataset of b-value 1000 have larger scales than that from the b-value 2000 dataset, which was expected. The shape differences are conveyed in terms of the checkerboard style edge differences. With the single hue colormap, it is difficult to perceive shape differences for tensors of similar scales. Figure 11e shows the Tender glyphs with the dual hue colormap which is more suitable for distinguishing two tensors with similar scales. A closeup of the Tender glyphs within the area marked as the rectangle in Figure 11e is shown in Figure 11f in the view-aligned projection style of the first and second normalized eigenvalues. Even the subtle differences, for example for the linear tensors, can be efficiently identified.

The feature space selection can be used to find regions with large differences or outliers. The locations with both large shape and orientation differences are selected, as shown in Figure 12a, while the corresponding feature space is shown at the top left corner. It can be seen from Figure 12b that most of the Tender glyphs are shown at the bottom of the DTI volume, which are probably in uninteresting regions for analysis. However, there are two groups of glyphs located inside the volume, as marked by the white rectangles in Figure 12a. Figure 12b shows a view of some of these normalized glyphs located on one coronal slice. Figure 12c presents a view for this region without

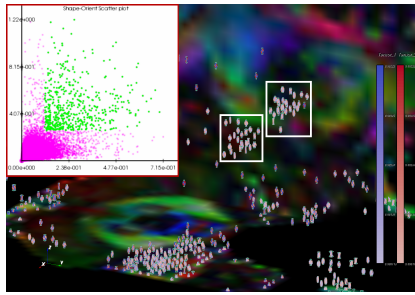
encoding the tensor scales. The shape differences become more obvious via the Tender glyphs, and they can be more accurately assessed.

As another example of DTI dataset comparison the Tender glyph is applied to compare a DTI dataset from a healthy subject and from an HIV-infected subject. The datasets were pre-registered through FSL². The size of each dataset is $112 \times 112 \times 55$ with an isotropic resolution of 2mm. Two regions of the corpus callosum (CC) on a sagittal slice are selected as the ROIs shown as white rectangles in Figure 13a. Blue represents the DTI dataset of a healthy subject, while red is for the DTI dataset from an HIV-infected subject. Figure 13c clearly shows the orientation differences, compared to the superposed tensor glyphs shown in Figure 13b. Voxels with consistent orientation differences are more efficiently recognized in the posterior region of the CC. Figure 13d, 13e, and 13f show the visualization results for the anterior region of the CC. From Figure 13e and 13f we can see that the orientations in the anterior region do not change a lot, but their shapes do. The view-aligned style of the Tender glyphs in Figure 13f further confirms that tensors of the HIV dataset are less linearly shaped in the indicated region. Further studies are necessary to see whether these findings remain consistent between larger populations.

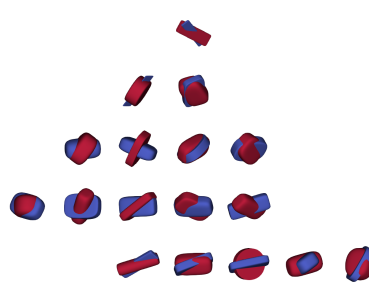
8 CONCLUSIONS AND FUTURE WORK

A glyph-based comparative visualization for diffusion tensor datasets is presented. We decompose the overall tensor differences into differences in shape, scale, and orientation, which have special interpretations for the consequences in the underlying tissue. We design a novel glyph, i.e., the Tender glyph to encode and visually present them in an easy-to-interpret way. The Tender glyph is composed of two superquadratic glyphs arranged in a checkerboard style that is efficient for the visual comparison of tensor shapes. The individual tensor scales or the scale differences are color-encoded, and we also design two colormaps, each of which has its own advantages for certain purposes. The arcs encode the orientation differences, which are intuitive and pre-attentive for perception. We build a feature space that is helpful for the interactive exploration and selection of relevant features. We

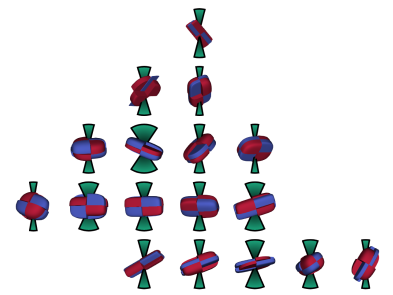
²<http://fsl.fmrib.ox.ac.uk/fsl/fslwiki/>



(a) Find interesting areas with both large shape and orientation differences via feature space.

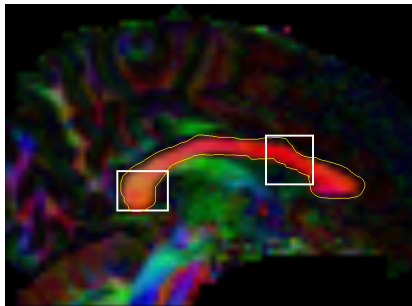


(b) Superposed superquadric tensor glyphs.

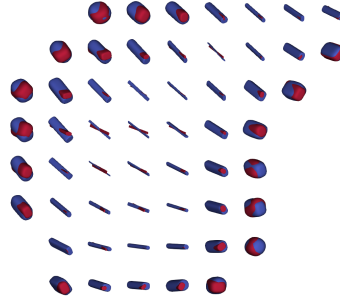


(c) The Tender glyphs clearly show the orientation and shape differences in detail.

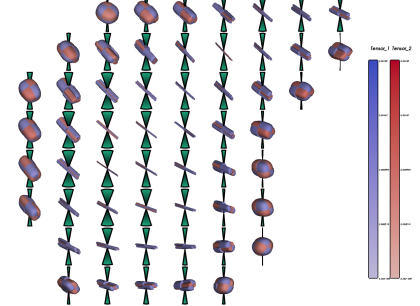
Fig. 12. Feather space filtering together with the Tender glyphs enable a detailed comparison at interesting areas.



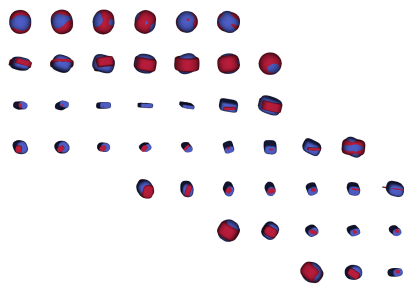
(a) Two ROIs selected on the CC.



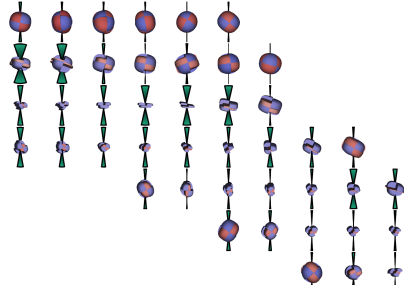
(b) Superposed superquadric tensor glyphs at the posterior area of CC.



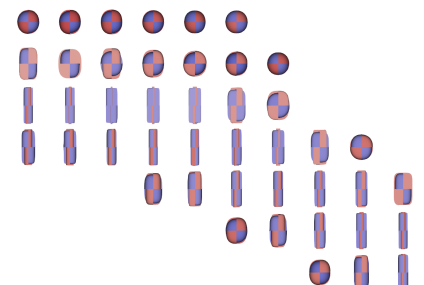
(c) Tender glyphs reveal consist orientation differences at the posterior area of CC.



(d) Superposed superquadric tensor glyphs at the anterior area of CC.



(e) Tender glyphs at the anterior area of CC, aligned with the blue dataset.



(f) Tender glyphs at the anterior area of CC with view-align projection style.

Fig. 13. The Tender glyphs clearly reveal the change of dominant tensor differences in different regions of CC.

present an initial user study that shows that the Tender glyph allows a more accurate and effective analysis for orientation and shape differences, although it does not improve the time performance in all tasks. Two cases based on brain DTI datasets illustrate the potential of the Tender glyph in comparative analysis of real-world datasets.

In the future, we would like to carry out a more exhaustive user study in a specific DTI application domain as well as a general evaluation of the Tender glyph in the way presented in Demiralp et al. [10].

Furthermore, the most well-known problem for the single tensor model is that it fails to model complex fiber configurations inside a voxel such as fiber crossings. More sophisticated modeling techniques such as HARDI can be used to describe those complex situations. How to extend the design idea of Tender glyph to HARDI is an open problem. The Tender glyph is currently only for pair-wise comparison. Though in the case study with the HIV dataset we compare two individual subjects from two groups, the Tender glyph can be applied to visualize the differences between the corresponding group means for inter-group comparison. Furthermore, in practice there are situations where multiple datasets need to be compared rather than just two. Therefore, another open problem is how to extend the Tender glyph

for comparison beyond two datasets. The underlying uncertainty of DTI [6], which is caused by the noise and the incomplete modeling, is another motivation for multiple DTI datasets comparison.

ACKNOWLEDGMENTS

The authors would like to thank Dr. Itamar Ronen (C.J.Gorter Center for High-field MRI, Leiden University Medical Center) for providing the DTI datasets with two different b-values. The HIV dataset was provided by the AGEhIV cohort study group and Co-morbidity in Relation to AIDS (COBRA) project. The control subject was provided by the Municipal Health Service Amsterdam. The authors would also like to thank Jianfei Yang and Joor Arkesteijn (Quantitative Imaging Group, Delft University of Technology) for their valuable feedback during the glyph design process. Kai Lawonn was partially funded by the BMBF (STIMULATE-OVGU: 13GW0095A).

REFERENCES

- [1] A. Abbasloo, V. Wiens, M. Hermann, and T. Schultz. Visualizing tensor normal distributions at multiple levels of detail. *IEEE Transactions on Visualization and Computer Graphics (Proceedings of the Visual Analytics*

- Science and Technology / Information Visualization / Scientific Visualization 2015*, 22(1), January 2016.
- [2] V. Arsigny, P. Fillard, X. Pennec, and N. Ayache. Log-Euclidean metrics for fast and simple calculus on diffusion tensors. *Magnetic Resonance in Medicine*, 56(2):411–421, 2006.
 - [3] Y. Assaf, D. Ben-Bashat, J. Chapman, S. Peled, I. Biton, M. Kafri, Y. Segev, T. Hendler, A. Korczyn, M. Graif, and Y. Cohen. High b-value q-space analyzed diffusion-weighted MRI: Application to multiple sclerosis. *Magnetic Resonance in Medicine*, 47(1):115–126, 2002.
 - [4] D. B. Bashat, L. B. Sira, M. Graif, P. Pianka, T. Hendler, Y. Cohen, and Y. Assaf. Normal white matter development from infancy to adulthood: Comparing diffusion tensor and high b value diffusion weighted MR images. *Journal of Magnetic Resonance Imaging*, 21(5):503–511, 2005.
 - [5] P. J. Basser, J. Mattiello, and D. LeBihan. MR diffusion tensor spectroscopy and imaging. *Biophysical Journal*, 66(1):259–267, 1994.
 - [6] T. Behrens, M. Woolrich, M. Jenkinson, H. Johansen-Berg, R. Nunes, S. Clare, P. Matthews, J. Brady, and S. Smith. Characterization and propagation of uncertainty in diffusion-weighted mr imaging. *Magnetic Resonance in Medicine*, 50(5):1077–1088, 2003.
 - [7] Ø. Bergmann, G. Kindlmann, A. Lundervold, and C.-F. Westin. Diffusion k-tensor estimation from Q-Ball imaging using discretized principal axes. In *Proc. Medical Image Computing and Computer-Assisted Intervention (MICCAI)*, pages 268–275, 2006.
 - [8] R. Borgo, J. Kehler, D. H. Chung, E. Maguire, R. S. Laramée, H. Hauser, M. Ward, and M. Chen. Glyph-based visualization: Foundations, design guidelines, techniques and applications. *Eurographics State of the Art Reports*, pages 39–63, 2013.
 - [9] S. Busking, C. P. Botha, L. Ferrarini, J. Milles, and F. H. Post. Image-based rendering of intersecting surfaces for dynamic comparative visualization. *The Visual Computer*, 27(5):347–363, 2011.
 - [10] Ç. Demiralp, C. E. Scheiddegger, G. L. Kindlmann, D. H. Laidlaw, and J. Heer. Visual embedding: A model for visualization. *IEEE Computer Graphics and Applications*, 2014.
 - [11] D. H. Chung, P. A. Legg, M. L. Parry, R. Bown, I. W. Griffiths, R. S. Laramée, and M. Chen. Glyph sorting: Interactive visualization for multi-dimensional data. *Information Visualization*, 14(1):76–90, 2015.
 - [12] M. J. DaSilva, S. Zhang, C. Demiralp, and D. H. Laidlaw. Visualizing the differences between diffusion tensor volume images. In *Proceedings of the International Society for Magnetic Resonance in Medicine Diffusion MRI Workshop*, 2000.
 - [13] M. de Groot, M. A. Ikram, S. Akoudad, G. P. Krestin, A. Hofman, A. van der Lugt, W. J. Niessen, and M. W. Vernooij. Tract-specific white matter degeneration in aging: The Rotterdam Study. *Alzheimer's & Dementia*, 11(3):321–330, 2015.
 - [14] D. B. Ennis and G. Kindlmann. Orthogonal tensor invariants and the analysis of diffusion tensor magnetic resonance images. *Magnetic Resonance in Medicine*, 55(1):136–146, 2006.
 - [15] P. T. Fletcher and S. Joshi. Riemannian geometry for the statistical analysis of diffusion tensor data. *Signal Processing*, 87(2):250–262, 2007.
 - [16] M. Gleicher, D. Albers, R. Walker, I. Jusufi, C. D. Hansen, and J. C. Roberts. Visual comparison for information visualization. *Information Visualization*, 10(4):289–309, 2011.
 - [17] K. M. Hasan, D. L. Parker, and A. L. Alexander. Comparison of gradient encoding schemes for diffusion-tensor MRI. *Journal of Magnetic Resonance Imaging*, 13(5):769–780, 2001.
 - [18] I. Hotz, J. Sreevalsan-Nair, H. Hagen, and B. Hamann. Tensor field reconstruction based on eigenvector and eigenvalue interpolation. In *Scientific Visualization: Advanced Concepts*, volume 1 of *Dagstuhl Follow-Ups*, pages 110–123, 2010.
 - [19] D. K. Jones. The effect of gradient sampling schemes on measures derived from diffusion tensor MRI: A Monte Carlo study. *Magnetic Resonance in Medicine*, 51(4):807–815, 2004.
 - [20] D. K. Jones, L. D. Griffin, D. C. Alexander, M. Catani, M. A. Horsfield, R. Howard, and S. C. Williams. Spatial normalization and averaging of diffusion tensor MRI data sets. *Neuroimage*, 17(2):592–617, 2002.
 - [21] G. Kindlmann. Superquadric tensor glyphs. In *Proceedings of the Sixth Joint Eurographics/IEEE TCVG Symposium on Visualization*, pages 147–154, 2004.
 - [22] G. Kindlmann, D. Ennis, R. Whitaker, and C.-F. Westin. Diffusion tensor analysis with invariant gradients and rotation tangents. *IEEE Transactions on Medical Imaging*, 26(11):1483–1499, 2007.
 - [23] G. Kindlmann, R. S. J. Estepar, M. Niethammer, S. Haker, and C.-F. Westin. Geodesic-loxodromes for diffusion tensor interpolation and difference measurement. In *Medical Image Computing and Computer-Assisted Intervention—MICCAI 2007*, pages 1–9. Springer, 2007.
 - [24] G. Kindlmann and C.-F. Westin. Diffusion tensor visualization with glyph packing. *IEEE Transactions on Visualization and Computer Graphics*, 12(5):1329–1336, 2006.
 - [25] P. Kok, M. Baiker, E. Hendriks, F. H. Post, J. Dijkstra, C. W. Löwik, B. P. Lelieveldt, and C. P. Botha. Articulated planar reformation for change visualization in small animal imaging. *IEEE Transactions on Visualization and Computer Graphics*, 16(6):1396–1404, 2010.
 - [26] A. Kratz, C. Auer, M. Stommel, and I. Hotz. Visualization and analysis of second-order tensors: Moving beyond the symmetric positive-definite case. *Computer Graphics Forum*, 32(1):49–74, 2013.
 - [27] M. Kubicki, H. Park, C. Westin, P. Nestor, R. Mulkern, S. Maier, M. Niznikiewicz, E. Connor, J. Levitt, M. Frumin, et al. DTI and MTR abnormalities in schizophrenia: analysis of white matter integrity. *Neuroimage*, 26(4):1109–1118, 2005.
 - [28] D. H. Laidlaw, E. T. Ahrens, D. Kremers, M. J. Avalos, R. E. Jacobs, and C. Readhead. Visualizing diffusion tensor images of the mouse spinal cord. In *Visualization '98. Proceedings*, pages 127–134. IEEE, 1998.
 - [29] A. E. Lie, J. Kehler, and H. Hauser. Critical design and realization aspects of glyph-based 3D data visualization. In *Proceedings of the 25th Spring Conference on Computer Graphics*, pages 19–26. ACM, 2009.
 - [30] T. Peeters, P. Rodrigues, A. Vilanova, and B. ter Haar Romeny. Analysis of distance/similarity measures for diffusion tensor imaging. In *Visualization and Processing of Tensor Fields*, pages 113–136. Springer, 2009.
 - [31] C. Pierpaoli and P. Basser. Toward a quantitative assessment of diffusion anisotropy. *Magnetic Resonance in Medicine*, 36(6):893–906, 1996.
 - [32] T. Ropinski, S. Oeltze, and B. Preim. Survey of glyph-based visualization techniques for spatial multivariate medical data. *Computers & Graphics*, 35(2):392–401, 2011.
 - [33] J. Schmidt, R. Preiner, T. Auzinger, M. Wimmer, M. E. Gröller, and S. Bruckner. YMCA-your mesh comparison application. In *2014 IEEE Conference on Visual Analytics Science and Technology (VAST)*, pages 153–162, 2014.
 - [34] T. Schultz and G. L. Kindlmann. Superquadric glyphs for symmetric second-order tensors. *IEEE Transactions on Visualization and Computer Graphics*, 16(6):1595–1604, 2010.
 - [35] T. Schultz, L. Schläpke, B. Schölkopf, and T. Schmidt-Wilcke. HiFiVE: A Hilbert space embedding of fiber variability estimates for uncertainty modeling and visualization. *Computer Graphics Forum*, 32(3):121–130, 2013.
 - [36] A. Schwartzman, R. F. Dougherty, and J. E. Taylor. Cross-subject comparison of principal diffusion direction maps. *Magnetic Resonance in Medicine*, 53(6):1423–1431, 2005.
 - [37] R. Stokking, I. G. Zubal, and M. A. Viergever. Display of fused images: methods, interpretation, and diagnostic improvements. *Seminars in Nuclear Medicine*, 33(3):219–227, July 2003.
 - [38] D. S. Tuch. *Diffusion MRI of complex tissue structure*. PhD thesis, Harvard University, 2002.
 - [39] R. van Pelt, R. Gasteiger, K. Lawonn, M. Meuschke, and B. Preim. Comparative blood flow visualization for cerebral aneurysm treatment assessment. *Computer Graphics Forum*, 33(3):131–140, 2014.
 - [40] V. Verma and A. Pang. Comparative flow visualization. *IEEE Transactions on Visualization and Computer Graphics*, 10(6):609–624, 2004.
 - [41] C.-F. Westin, S. E. Maier, B. Khidir, P. Everett, F. A. Jolesz, and R. Kikinis. Image processing for diffusion tensor magnetic resonance imaging. In *Medical Image Computing and Computer-Assisted Intervention—MICCAI '99*, pages 441–452, 1999.
 - [42] C.-F. Westin, S. Peled, H. Gudbjartsson, R. Kikinis, and F. A. Jolesz. Geometrical diffusion measures for MRI from tensor basis analysis. In *ISMRM '97*, page 1742, April 1997.
 - [43] Y. Wu, P. Storey, B. Cohen, L. Epstein, R. Edelman, and A. Ragin. Diffusion alterations in corpus callosum of patients with HIV. *American journal of neuroradiology*, 27(3):656–660, 2006.